sciendo

CuO–WATER MHD MIXED CONVECTION ANALYSIS AND ENTROPY GENERATION MINIMIZATION IN DOUBLE-LID–DRIVEN U-SHAPED ENCLOSURE WITH DISCRETE HEATING

Bouchmel MLIKI*, Rached MIRI*, Ridha DJEBALI, Mohamed A. ABBASSI***

*Research Lab, Technology Energy and Innovative Materials, Faculty of Sciences, University of Gafsa, Gafsa 2112, Tunisia
**UR22ES12: Modeling Optimization and Augmented Engineering, ISLAIB, University of Jendouba, Beja 9000, Tunisia

bouchmelmliki@hotmail.com, rachedmiri111@gmail.com, jbelii_r@hotmail.fr, abbassima@gmail.com

received 10 August 2022, revised 14 November 2022, accepted 30 November 2022

Abstract: The present study explores magnetic nanoliquid mixed convection in a double lid–driven U-shaped enclosure with discrete heating using the lattice Boltzmann method (LBM) numerical method. The nanoliquid thermal conductivity and viscosity are calculated using the Maxwell and Brinkman models respectively. Nanoliquid magnetohydrodynamics (MHD) and mixed convection are analyzed and entropy generation minimisation has been studied. The presented results for isotherms, stream isolines and entropy generation describe the interaction between the various physical phenomena inherent to the problem including the buoyancy, magnetic and shear forces. The operating parameters' ranges are: Reynolds number ($\mathrm{Re}: 1-100$), Hartman number ($\mathrm{Ha}: 0-80$), magnetic field inclination ($\gamma: 0°-90°$), nanoparticles volume fraction ($\phi: 0-0.04$) and inclination angle ($\alpha: 0°-90°$). It was found that the N_{um} and the total entropy generation augment by increasing Re, ϕ: and γ. conversely, an opposite effect was obtained by increasing Ha and α. The optimum magnetic field and cavity inclination angles to maximum heat transfer are $\gamma = 90°$ and $\alpha = 0$.

Key words: U-shaped enclosure, MHD mixed convection, nanoliquid, double lid-driven cavity, entropy generation, LBM

1. INTRODUCTION

Nanoliquid mixed convection in different geometries has elicited attention and interest from many researchers due to its availability in nature and its numerous engineering applications including in electronic equipment cooling, polymer industry, heat exchangers, automobile radiators and space technology [1–13]. Mixed convective heat transfer in enclosures has been extensively investigated during the last decades [14–17]. Mliki et al. [14] studied mixed convection in a lid-driven square cavity filled with copper–water nanofluid. They discussed the influences of volumetric fraction of nanoparticles (ϕ), Rayleigh number (Ra) and Reynolds numbers (Re) on the fluid flow, heat transfer and S_{gen}. Their results showed that the Nu_m and S_{gen} augment as the Rayleigh and Reynolds numbers. Also, they found that the addition of nanoparticles in pure water leads to enhancement of heat transfer rate. The results of Sheremet and Pop [15], who considered the same problem of mixed convection of nanoliquid in a lid-driven square cavity, concluded that the heat transfer was enhanced with the Richardson number. Besides, Nayak et al. [16] found that the addition of nanoparticles leads to enhancement of Nu_m for the mixed convection of Cu–water nanoliquid in a differentially heated cavity. Similarly, Sourtiji et al. [17] examined the mixed convection of nanoliquid in a ventilated cavity. Their results showed that the Nu_m augments with an increase in Reynolds number (Re), Richardson number (Ri) and nanoparticle volume fraction (ϕ). Additional papers on nanofluid mixed convection in cavities can also be found in the literature [18–21]. Aljabair et al. [20] reported a problem of mixed convection in a sinusoidal lid-driven cavity with non-uniform temperature distribution on the wall utilising nanofluid. Their results showed that heat transfer rate augments as the volumetric fraction of nanoparticles *(ϕ),* Reynolds number (Re) and Rayleigh number (Ra).

The effect of an external magnetic field on convective heat transfer in different geometries was studied by many researchers [22–25]. Aljabair et al. [22] studied the natural convection heat transfer in corrugated annuli with H_2O–Al_2O_3 nanofluid. They reported an enhancement in heat transfer by augment of the Rayleigh number and nanoparticles volume fraction. As similar finding has been observed by Mahmoudi et al. [23], who considered the magnetic field effect on natural convection in a square cavity filled with Al_2O_3–water nanoliquid and inferred that convective heat transfer was reduced by an increase in external magnetic field intensity (Ha). In another paper, Mliki et al. [24] studied the magneto-hydrodynamic (MHD) laminar convection in a linearly/sinusoidally heated cavity with a CuO–water nanoliquid using the lattice Boltzmann method (LBM). They analysed the effect of Rayleigh number (Ra), Hartmann number (Ha), heat generation or absorption coefficient (Ra) and nanoparticle volume concentration (ϕ) on the fluid flow and heat transfer. They concluded that the heat transfer rate increased when the role of Brownian motion of nanoparticles was considered. The influence of volumetric fraction of nanoparticles (ϕ), aspect ratios (AR) and Richardson number (Ri) on heat transfer and fluid movement of a hybrid H_2O–Cu–Al_2O_3 nanofluid in a multi-lid–driven concentric trapezoidal annulus has been investigated by Alesbe et al. [25]. The results indicate that the heat transfers' skin friction increases with increase in the volume fraction of nanoparticles. Additionally, the maximum stream function value increases with increase in the aspect ratio and the volume fraction of hybrid nanofluid.

For the case of mixed convection flows, the effect of magnetic field indifferent configurations has been extensively investigated [26–29]. Hussain et al. [26] studied the mixed convection and S_{gen} in a two-dimensional double-lid–driven square cavity. They discussed the influences of volumetric fraction of nanoparticles (ϕ), Reynolds numbers (Re), Hartman number (Ha), Richardson number (Ri) and inclined magnetic field (γ) on the fluid flow, heat transfer and S_{gen}. The results indicate that the heat transfers and S_{gen} augment with the Richardson number (Ri) and Reynolds number (Re). Also, they concluded that with the increment in the solid volume fraction of nanofluids (ϕ), S_{gen} decreases. Shirvan et al. [27] numerically analysed the MHD effect on a mixed convection in a ventilated square cavity. Their results showed that the heat transfer rate augments as the Hartmann number (Ha) increases. Pordanjani and Aghakhani [28] examined the natural convection and irreversibilities between two inclined concentric cylinders in the presence of a uniform magnetic field and radiation. They observed that the thermal performance and irreversibilities have increasing pursuant to the Rayleigh number, hot pipe diameter and addition of more nanopowder. In another paper, Aghakhani et al. [29] have discussed the entropy generation and exergy analysis of Ag–MgO/water hybrid nanofluid within a circular heatsink with different numbers of outputs. They reported that an enhancement in the Re leads to a reduction in the exergy loss as well as the first and second law efficiencies.

Previous investigations have focused predominantly on investigating heat transfer by nanofluids mixed convectively with and without a magnetic field in regular geometries under uniform heating. In the present work, the nanoliquid mixed convection was considered with the associated S_{gen} in a double-lid–driven U-shaped enclosure with discrete heating under an external magnetic field. The interaction between the induced shear, buoyancy and magnetic forces was worthy of investigation, the objective being to evaluate its impact on the heat transfer and S_{gen} rates. Results are based on visualisation of the flow, thermal fields, local S_{gen}, Nu_m and total S_{gen}.

2. PROBLEM STATEMENT

The studied problem configuration was a two-dimensional double-lid–driven U-shaped enclosure with discrete heating and filled with nanoliquid, as illustrated in Fig. 1.

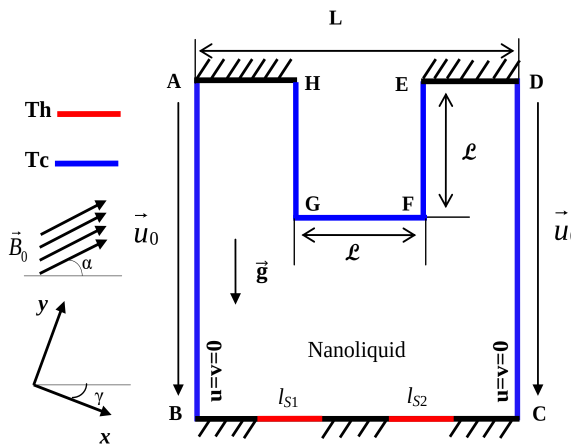

Fig. 1. Geometry of the problem

Two constant temperature heat sources of length L/5 are located at the bottom wall (Th). The walls (AB, CD, EF, FG and GH) are maintained at cold temperature Tc. The cavity aspect ratio was AR = L/L = 0.4.

The inclination of magnetic field ($\vec{B}$) and that of the cavity are γ and α, respectively. The two vertical walls (AB and DC) move downward at constant velocity Uo. Such a configuration leads to a combined and complex interaction between various effects within the cavity, including the buoyancy and shear forces and the magnetic field.

The fluid in the U-shaped enclosure is a nanoliquid (CuO–water) (Tab. 1) [30]. The density divergence in the nanoliquid was approximated by the regular Boussinesq approximation.

Tab. 1. Thermophysical properties of liquid and nanoparticles [30]

Thermophysical properties	H2O	CuO
C_p ($J \cdot kg^{-1} \cdot K^{-1}$)	4,179	540
ρ ($kg \cdot m^{-3}$)	997.1	6,500
k ($W \cdot m^{-1} \cdot K^{-1}$)	0.631	18
$\beta \times 10^{-5}$(1/K)	21	0.85
σ $(\Omega m)^{-1}$	0.05	$2.7 \cdot 10^{-8}$

3. GOVERNING EQUATIONS

By applying a magnetic field, the governing equations for mixed convection in the two-dimensional double-lid–driven U-shaped enclosure can be obtained as follows [31]:

$$\frac{\partial U}{\partial X}+\frac{\partial V}{\partial Y}=0 \quad (1)$$

$$U\frac{\partial U}{\partial X}+V\frac{\partial U}{\partial Y}=-\frac{\partial P}{\partial X}+\frac{1}{Re}\frac{\rho_f}{\rho_{nf}}\frac{1}{(1-\varphi)^{2.5}}\left(\frac{\partial^2 U}{\partial X^2}+\frac{\partial^2 U}{\partial Y^2}\right)+ \frac{\rho_f}{\rho_{nf}}\frac{\sigma_{nf}}{\sigma_f}\frac{Ha^2}{Re}(V\sin\gamma\ \cos\gamma-U\cos^2\gamma)+ Ri\frac{\rho_f}{\rho_{nf}}\left(1-\varphi+\frac{(\rho\beta)_p}{(\rho\beta)_f}\right)\theta\ \sin\alpha \quad (2)$$

$$U\frac{\partial V}{\partial X}+V\frac{\partial V}{\partial Y}=-\frac{\partial P}{\partial X}+\frac{1}{Re}\frac{\rho_f}{\rho_{nf}}\frac{1}{(1-\varphi)^{2.5}}\left(\frac{\partial^2 V}{\partial X^2}+\frac{\partial^2 V}{\partial Y^2}\right)+ \frac{\rho_f}{\rho_{nf}}\frac{\sigma_{nf}}{\sigma_f}\frac{Ha^2}{Re}(U\sin\gamma\ \cos\gamma-V\cos^2\gamma)+ Ri\frac{\rho_f}{\rho_{nf}}\left(1-\varphi+\frac{(\rho\beta)_p}{(\rho\beta)_f}\right)\theta\ \cos\ \alpha \quad (3)$$

$$U\frac{\partial\theta}{\partial X}+V\frac{\partial\theta}{\partial Y}=\frac{\alpha_{nf}}{\alpha_f}\frac{1}{Re\ Pr}\left(\frac{\partial^2\theta}{\partial X^2}+\frac{\partial^2\theta}{\partial Y^2}\right) \quad (4)$$

where σ_{nf}, β, γ and α are the nanoliquid thermal diffusivity, the thermal expansion coefficient, inclined magnetic field and inclination angle of the cavity, respectively.

The dimensionless Sgen for the case of MHD nanoliquid mixed convection flow is given by [26]:

$$S_T=\frac{k_{nf}}{k_f}\left[\left(\frac{\partial\theta}{\partial X}\right)^2+\left(\frac{\partial\theta}{\partial Y}\right)^2\right]+ \chi\frac{\mu_{nf}}{\mu_f}\left[2\left(\frac{\partial U}{\partial X}\right)^2+2\left(\frac{\partial V}{\partial Y}\right)^2+\left(\frac{\partial U}{\partial Y}+\frac{\partial V}{\partial X}\right)^2\right] +\chi Ha^2\frac{\sigma_{nf}}{\sigma_f}(U\sin\gamma\ \ -V\cos\gamma)^2 \quad (5)$$

where Sgen,h, Sgen,v and Sgen,M are the Sgen due to heat

DOI 10.2478/ama-2023-0013

transport, Sgen due to fluid friction and Sgen due to application of the magnetic field, respectively. The irreversibility factor χ was expressed by:

$$\chi = \frac{\mu_f T_0}{k_f}\left(\frac{U_0}{T_h - T_c}\right)^2 \quad (6)$$

The average Sgen was calculated by:

$$S_{avr} = \frac{1}{V}\int_V S_T dV \quad (7)$$

where V was the total volume of the physical domain.

The dimensionless boundary conditions are calculated as follows: Cold walls AB, CD, EF, FG, GH: U = V = 0, θ = 0; Hot walls (0.2 ≤ IS1 ≤ 0.4) and (0.6 ≤ IS2 ≤ 0.8): θ = 1; Adiabatic walls (0 ≤ X < 0.2), (0.4 < X < 0.6) and (0.8 < X ≤ 1): $\partial T/\partial Y = 0$.

The local and integral Nu along the two heat sources (IS1, IS2) can be obtained as:

$$Nu = -\frac{k_{nf}}{k_f}\left(\frac{\partial\theta}{\partial Y}\right)\Big|_{Y=0} \quad (8)$$

$$\overline{Nu}_{I_{S_1}} = \int_{0.2}^{0.4} Nu\, dX \quad , \quad Nu_{I_{S_2}} = \int_{0.6}^{0.8} Nu\, dX \quad (9)$$

Effective density, specific heat capacity, thermal expansion coeffi-cient and thermal diffusivity of the nanoliquid are, respectively, expressed as follows [32, 33]:

$$\rho_{nf} = (1-\varphi)\rho_f + \varphi\rho_p \quad (10)$$

$$(\rho C_p)_{nf} = (1-\varphi)(\rho C_p)_f + \varphi(\rho C_p)_p \quad (11)$$

$$(\rho\beta)_{nf} = (1-\varphi)(\rho\beta)_f + \varphi(\rho\beta)_p \quad (12)$$

$$\alpha_{nf} = \frac{k_{nf}}{(\rho C_p)_{nf}} \quad (13)$$

The thermal conductivity and the electrical conductivity of the nanoliquid are, respectively, calculated as follows [34, 35]:

$$k_{static} = k_f \frac{k_P + 2k_f - 2\varphi(k_f - k_P)}{k_P + 2k_f + \varphi(k_f - k_P)} \quad (14)$$

$$\frac{\sigma_{nf}}{\sigma_f} = 1 + \frac{3\left(\frac{\sigma_s}{\sigma_f} - 1\right)\varphi}{\left(\frac{\sigma_s}{\sigma_f} + 2\right) - \left(\frac{\sigma_s}{\sigma_f} - 1\right)\varphi} \quad (15)$$

Nanoliquid effective dynamic viscosity was calculated using the Brinkman model [36]

$$\mu_{static} = \frac{\mu_f}{(1-\varphi)^{2.5}} \quad (16)$$

4. NUMERICAL METHOD

4.1. Brief introduction to LBM

The LBM was based on Ludwig Boltzmann's kinetic theory of gases. The fundamental idea is that gases/fluids can be a large number of small particles moving with random motions. The exchange of momentum and energy is achieved through particle streaming and collision.

The dimensionless equations were solved by using LBM, which employs Boltzmann's kinetic theory of gases [26]. By Bhatnagar–Gross Krook approximation, LBM was based on two distribution functions g and f of the temperature and flow fields in this study, respectively.

$$f_i(x + c_i\Delta t, t + \Delta t) = f_i(x,t) - \frac{1}{\tau_v}\left(f_i(x,t) - f_i^{eq}(x,t)\right) + \Delta t c_i F_i \quad (17)$$

$$g_i(x + c_i\Delta t, t + \Delta t) = g_i(x,t) - \frac{1}{\tau_a}\left(g_i(x,t) - g_i^{eq}(x,t)\right) \quad (18)$$

where Δt denotes the lattice time, lattice relaxation time for the flow and temperature fields, respectively. Two local equilibrium distribution functions for the temperature and flow fields g_i^{eq} and f_i^{eq} are calculated with Eqs (19) and (20) [37]:

$$f_i^{eq} = w_i r\left[1 + \frac{3(c_i.u)}{c^2} + \frac{9(c_i.u)^2}{2c^4} - \frac{3u^2}{2c^2}\right] \quad (19)$$

$$g_i^{eq} = w_i' T\left[1 + 3\frac{c_i.u}{c^2}\right] \quad (20)$$

The nine velocities (D2Q9) lattice model (Fig. 2) was used in the present study with a uniform grid size of dx = dy for simulating the steady MHD mixed convection of nanoliquid.

According to this model, the weighting factors wi and the discrete particle velocity vectors ci can be defined as follows [38]:

$$w_0 = \frac{4}{9}, w_i = \frac{1}{9} for i = 1,2,3,4 \quad and \quad w_i = \frac{1}{36} \; for \;\; i = 5,6,7,8 \quad (21)$$

$$c_i = \begin{cases} 0 & i = 0 \\ (cos[(i-1)\pi/2], sin[(i-1)\pi/2])c & i = 1,2,3,4 \\ \sqrt{2}(cos[(i-5)\pi/2 + \pi/4], sin[(i-5)\pi/2 + \pi/4])c & i = 5,6,7,8 \end{cases} \quad (22)$$

Finally, macroscopic variables (ρ, u and T) are calculated using the following equations:

$$\rho = \sum_i f_i, \qquad \rho u = \sum_i f_i \mathbf{c_i}, \qquad T = \sum_i g_i \quad (23)$$

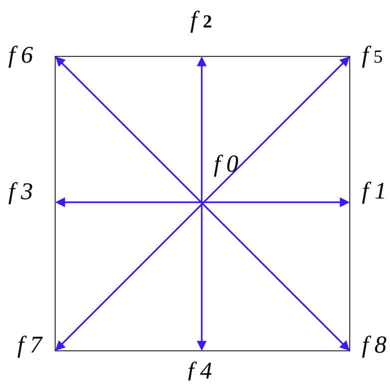

Fig. 2. Direction of streaming velocities, D2Q9

5. MESH VERIFICATION AND VALIDATION

Tab. 2 shows the calculated Num at different mesh sizes for the case: nanoliquid (Cu–water) with Re = 50; Ri = 20; ϕ = 0.04; Ha = 30; α = 45°; and γ = 0 (50 × 50, 75 × 75, 100 × 100 and 150 × 150 nodes). It was found that the variation of the Num between 100 × 100 and 150 × 150 grids was <0.005095. However, for all calculations in this numerical study, the 100 × 100 uniform grid was employed.

sciendo
DOI 10.2478/ama-2023-0013

Tab. 2. Grid independence test for Re = 50; Ri = 20; ϕ = 4 · 10^{-2}; Ha = 30; α = 45°; and γ = 0

Grid size	$\overline{Nu}_{ls_1}$	$\overline{Nu}_{ls_2}$
50 × 50	3.910183	4.072377
75 × 75	4.232592	4.389502
100 × 100	4.418533	4.575598
150 × 150	4.510627	4.580693

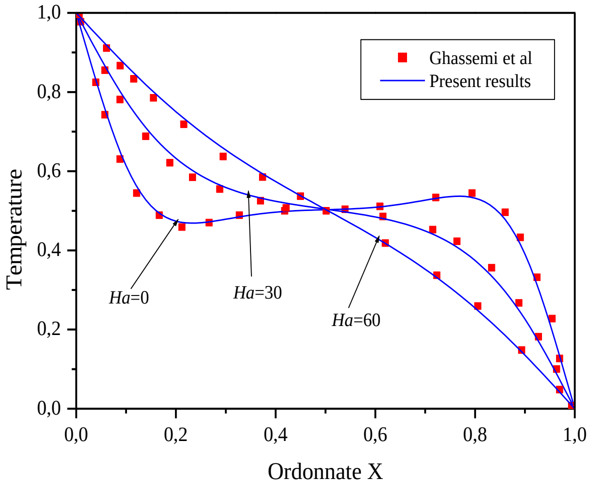

Fig. 3. Comparison of the temperature on axial midline between the present results and numerical results by Ghasemi et al. [39] (ϕ = 3 · 10–2 and Ra = 105)

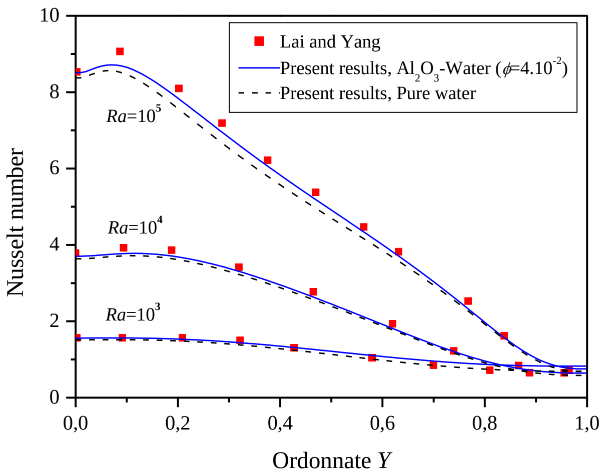

Fig. 4. Comparison of the local Nusselt number along the hot wall between the present results and numerical results by Lai and Yang [40]

For the validation of data, the present results are compared with the numerical results obtained by Ghasemi et al. [39] for the case of magnetic nanoliquid convection in a square enclosure (Fig. 3). In addition, a comparison of the local Nusselt number along the hot wall was made between the present results and the numerical results provided Lai and Yang [40] for the case of nanoliquid natural convection in a square enclosure (Fig. 4). The present numerical results have been also compared with those of Talebi et al. [41] for the case of mixed convection in a square lid-driven cavity (Fig. 5). Based on the aforementioned comparisons, the developed code was judged to be reliable for studying the MHD mixed convection of a nanoliquid confined in a double-lid–driven U-shaped enclosure with discrete heating under the effect of an external magnetic field.

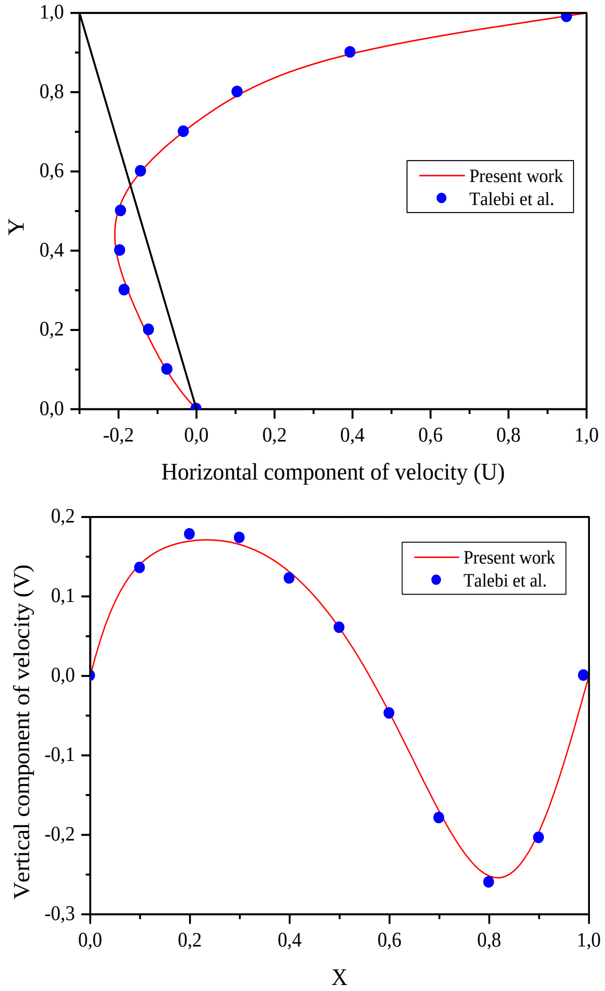

Fig. 5. Comparison of (a) horizontal component of velocity and (b) vertical component of velocity with those of de Talebi et al. [41] (Re = 100 and Ra = 1.47 · 104)

6. RESULTS AND DISCUSSION

The problem of two-dimensional MHD mixed convection in a double-lid–driven U-shaped enclosure containing a CuO–water nanoliquid was studied. The cavity aspect ratio was fixed at AR = 0.4. The effects of Reynolds number (1 ≤ Re ≤ 100), volume fraction of nanoparticles (0 ≤ ϕ ≤ 4 · 10^{-2}), Hartmann number (0 ≤ Ha ≤ 80), inclined magnetic field (0 ≤ γ ≤ 90°) and inclination angle of the cavity (0 ≤ α ≤ 90°) on the streamlines, local Sgen and heat transfer characteristics have been revealed.

6.1. Ifluuence of Reynolds number

Isotherms, local Sgen and streamlines of CuO–water nanoliquid for various Reynolds numbers are presented in this primary part of the numerical study for Ri = 30, γ = α = 0, Ha = 0 and ϕ = 0.04.

As can be seen from the streamlines in Fig. 6, for all Reynolds numbers, the flow structure, temperature contours and Sgen are

DOI 10.2478/ama-2023-0013

symmetrical about the vertical centerline (X = 0.5) of the heated U-shaped enclosure and are concentrated along the two heated sources (IS1 and IS2) due to enhanced fluid movement in these regions. Physically, this was true owing to the symmetrical boundary conditions about the horizontal X-axis (X = 0.5).

For low Reynolds numbers (Re = 1 and Re = 10), the fluid was well circulated in the top part of the cavity, and similarly for the density of the temperature distribution contours and local Sgen near the adiabatic walls (AH–ED). Moreover, the increase of the Reynolds number (Re = 50 and Re = 100) results in pushing the cold nanoliquid to the bottom corners (B and C), and consequently, the temperature patterns are compressed adjacently to the discrete heat sources (IS1 and IS2). This was a good reason for the increase in the value of the maximum stream function $|\psi|_{max}$ and the formation of active regions for Sgen. The cause of these changes was due to the increasing of heat transfer by the buoyancy force.

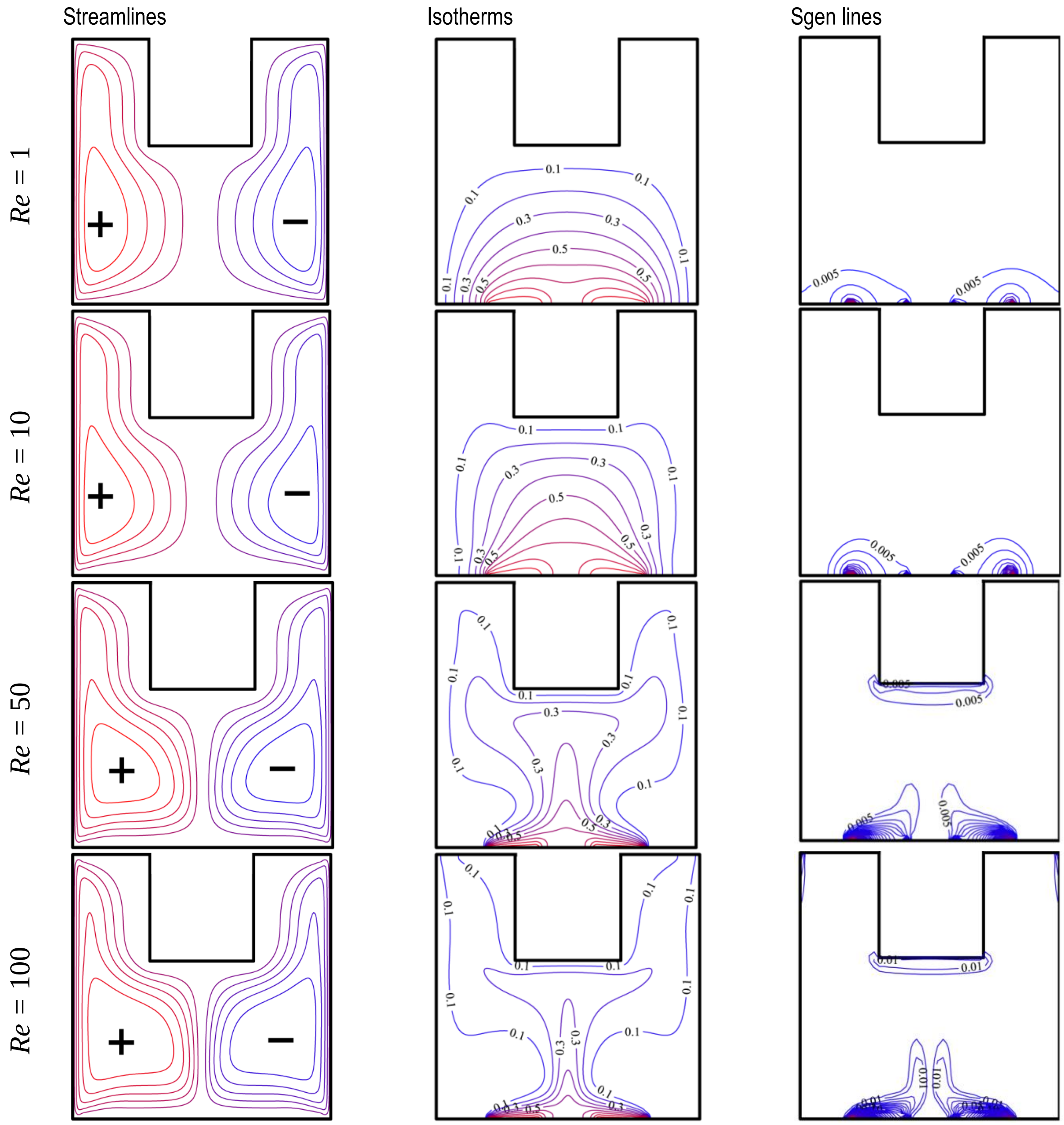

Fig. 6. Streamlines, isotherms and Sgen lines for different Re at Ri = 20, $\gamma = \alpha = 0$, Ha = 30 and $\phi = 4 \cdot 10^{-2}$

The effect of the Reynolds number on Sgen is shown in Tab. 3. It was observed that Sgen increases with an increase in Re due to the following factors: heat transfer SHT, fluid friction SFF, magnetic field SMF and total ST increase with an increase in Re. From this table, we may observe that the effect due to fluid friction and magnetic field has been negligible in comparison with that due to the heat transfer.

Tab. 3. Reynolds number effect on SHT, SFF, SMF and S at Ri = 20, $\gamma = \alpha = 0$, Ha = 30 and $\phi = 0.04$

	***Re* = 1**	***Re* = 10**	***Re* = 50**	***Re* = 100**
S_{HT}	2.75	3.44	9.13	12.2
S_{FF} (10^{-3})	2.91	3.06	3.31	3.77
S_{MF} (10^{-4})	4.33	4.49	5.23	5.84
S_T	2.753	3.443	9.133	12.204

Fig. 7a,b show the dependence of Num and total Sgen on the Reynolds numbers and solid concentration. By examining Eqs (14) and (21), an increase in solid concentration leads to a rise in the effective thermal conductivity. Accordingly, the maximum value of the Num and total Sgen are obtained at the maximum volumetric fraction of nanoparticles. In the case of low Reynolds numbers (Re=1 and Re=10), an increase in the solid concentration does not change the average Sgen and total Sgen. It was further observed that with the increase of the Reynolds number to Re = 50 and Re = 100, the difference between Nu (ϕ = 0) and Nu ($\phi = 4 \cdot 10^{-2}$) became faster. The variation of the total Sgen appears to be similar to the variation of Num; it was found to be increased by 11.65% when the volume fraction of nanoparticles passed from 0 to $4 \cdot 10^{-2}$ for Re = 100.

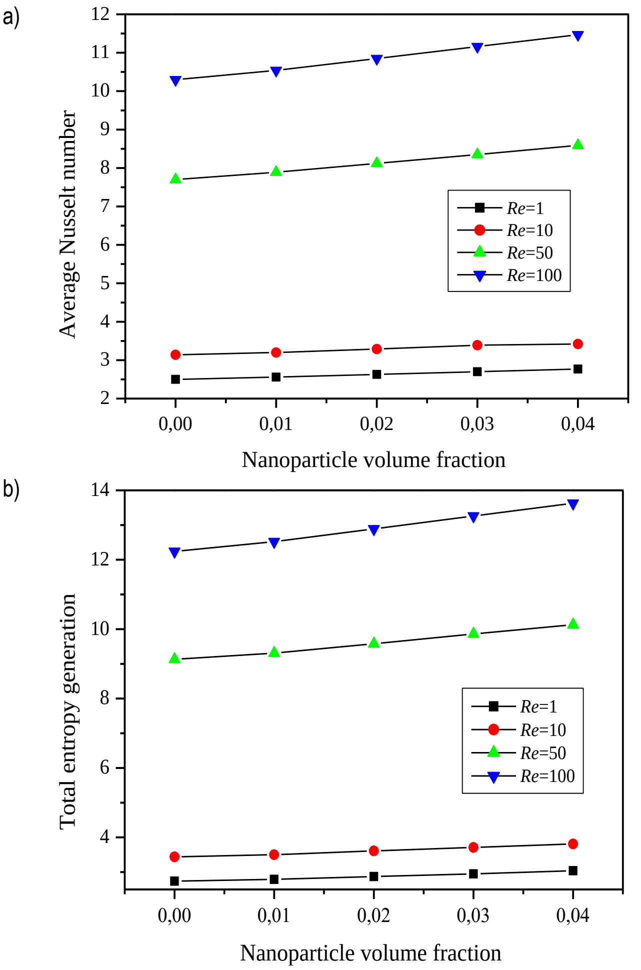

Fig. 7. Num (a) and total Sgen (b) for different values of the Reynolds numbers and volumetric fraction of nanoparticles at Ri = 20, γ = α = 0 and Ha = 30

6.2. Influence of Hartmann number

By an increase in Hartmann number (Ha), which results in a notable deterioration of the heat transfer. In fact, this can be explained by the fact that the effect of Lorentz force was opposite to the buoyancy force. It was observed that the increase in Hartmann number leads to a reduction of the flow intensity. The maximum values of the stream function equal $1.49 \cdot 10^{-1}$, $4.86 \cdot 10^{-1}$ and $2.78 \cdot 10^{-1}$ when those for Ha equal 0, 40 and 80, respectively. This can justify the observed decrease of the fluid motion and velocity. However, we note that the temperature distribution contours near the hot discrete sources are reduced as a result of the increase in the Lorentz forces. So, the presence of a magnetic field leads to substantial mixed convection flow dumping. The Ha effect on the local Sgen is displayed in Fig. 8. Increasing Hartmann number causes a reduction in the density of the local Sgen contours near the hot discrete sources. Accordingly, low Sgen values are obtained for high Ha values.

Fig. 9 (a,b) shows values of the Num and the total Sgen in the same conditions of Fig. 8 for various Hartmann numbers. The Num shown in Fig. 9(a) decreases by an increase in Hartmann number. We can explain the decrease of Num by referring to Eq. (9), which indicates that the effect of Lorentz force due to the application of an external magnetic field on heat transfer was opposite to the buoyancy force, and consequently, decreases the temperature gradients near the two heated sources (IS1 and IS2). Fig. 9(b) shows also that the behaviour of the total Sgen was similar to that of the Num.

The profiles of the dimensionless temperature in the heated U-shaped enclosure at y/L = 0.25 and y/L = 0.5 are depicted in Fig. 10(a,b). One can observe that the temperature in the U-shaped enclosure decreases by an increase in Hartmann number due to the reduction of the fluid movement and energy transferred by the discrete heat sources (IS1 and IS2). This explains the stagnation of the nanoliquid near the bottom part of the cavity for Ha = 80.

6.3. Influence of inclined magnetic field

The effects of a tilted magnetic field on the streamlines, isotherms and Sgen contours for inclination angles 0°, 30°, 60° and 90° are presented in Fig. 11. In the case of horizontal magnetic field (γ = 0), it can be seen that the streamlines contours are more clustered in the middle part of the U-shaped enclosure and are symmetrical about the vertical centreline (X = 0.5). Similarly, the temperature contours and Sgen are symmetrically distributed to the vertical centreline (X = 0.5). As γ increases to 30° and 60°, the circulation cell that was confined inside the right vertical portion of the U-shaped enclosure becomes stronger and the thermal boundary layer near the left moving walls (DE) becomes thicker. Moreover, as inclination angle α increases, the density of the Sgen distribution contours in the right part of the U-shaped enclosure grows. This is an indication of a higher heat transfer rate in this region. Finally, for γ = 90°, the flow, temperature contours and local Sgen are horizontally symmetric of the cavity and are concentrated along the two sources (IS1 and IS2). Consequently, the maximum heat flow occurs in the centre of the U-shaped enclosure.

Fig. 12 shows the impact of the inclination angle of magnetic field on Num. It was observed that at γ = 0; 90°, Num along the two heat sources (IS1, IS2) was the same. Num along the left heat source (IS1) decreases for γ ranging from 0° to 45° and then it decreases for γ = 60°–90°. On the other hand, the average heat transfer coefficient along the right heat source (IS2) increases considerably with increasing γ. This increase reaches 9.4% when γ changes from 0° to 90°. The Num maximum occurs at γ = 90°.

The effect of inclination angle of magnetic field on total Sgen is presented in Fig. 13. It was shown that the total Sgen slightly increases with the inclination angle for γ <45°. If the inclination angle was increased to 90°, the difference between ST (γ = 90°) and ST (γ = 0) becomes smaller. Consequently, a significant

DOI 10.2478/ama-2023-0013

effect of the inclination angle on the Sgen can be found for γ >45°.

6.4. Influence of inclination angle of the U-shaped enclosure

In this part, calculations are made for different inclination angles of the U-shaped enclosure α (Fig. 14). The volumetric fraction of nanoparticles was taken as $\phi = 4 \cdot 10^{-2}$, limiting the value of the validity of the Maxwell model.

For α = 0, two counter-rotating symmetric cells are formed inside the U-shaped cavity. Also, it was noticed that the temperature contours and Sgen are symmetrically distributed about the vertical centreline (X = 0.5) of the heated U-shaped enclosure. As γ increases, the circulation vortex that exists inside the left vertical portion of the cavity becomes stronger. The temperature patterns are compressed adjacently to the left moving walls (DE), and consequently, the density of the Sgen distribution grows in this region.

The effect of inclination angle of the U-shaped enclosure on the Num is depicted in Fig. 15. It was noticed that at γ = 0, the Num along the two heat sources (IS1, IS2) was the same. As α increased from 0° to 60°, the heat transfer due to left heat source S1 was enhanced. Conversely, an opposite effect associated with the Num behaviour can be found with an inclination angle of γ >60°. On the other hand, the heat transfer due to right heat source S2 decreases considerably with increasing γ. Generally, increasing α causes an increase of the Num, and consequently enhances the heat transfer process. The maximum value of the Num was 8.08 and occurs for α = 0. The variation of the total Sgen was similar to the variation of Num (Fig. 16).

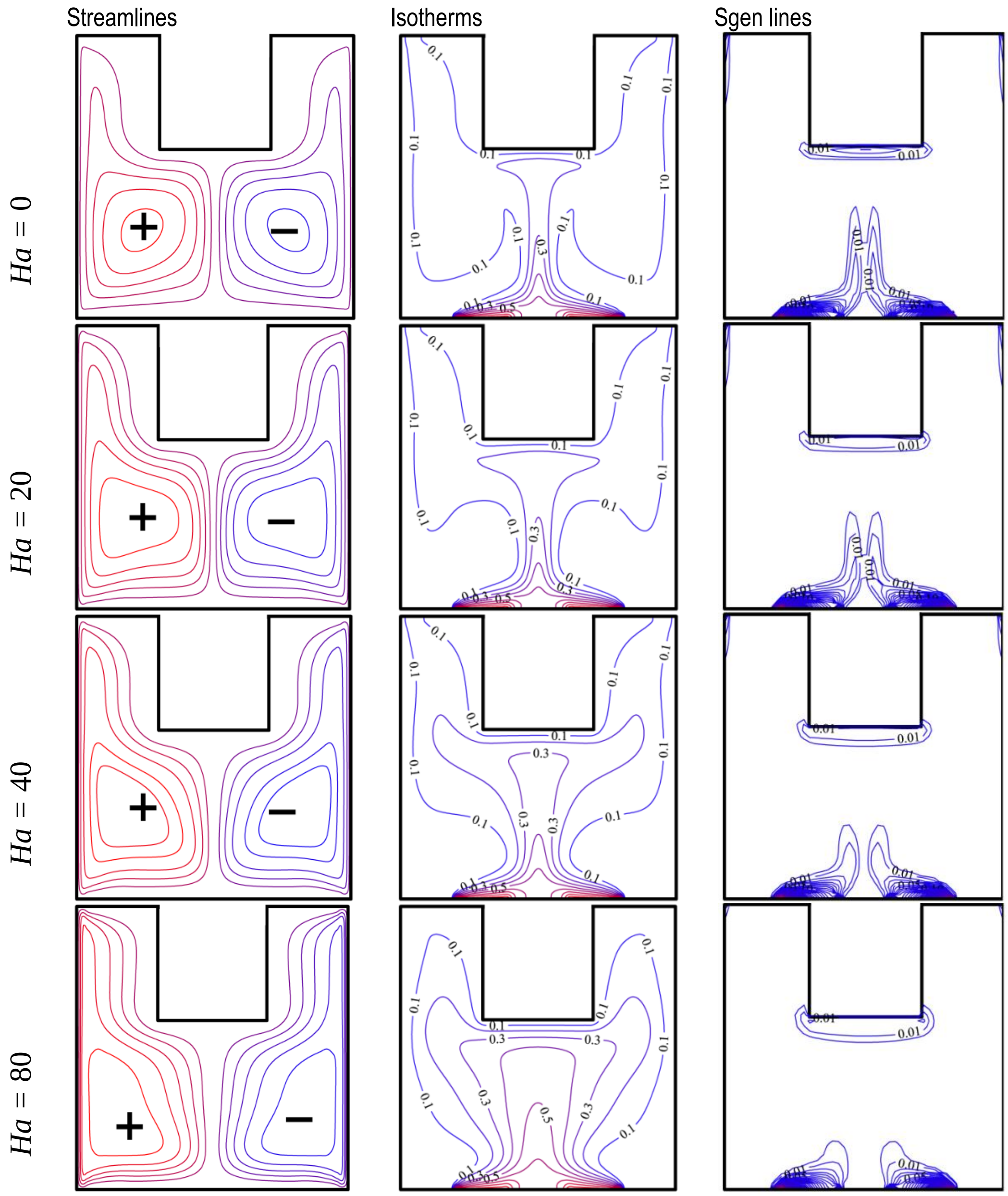

Fig. 8. Streamlines, isotherms and Sgen lines for different Ha at Re = 100, Ri = 20, γ = α = 0 and $\phi = 4 \cdot 10^{-2}$

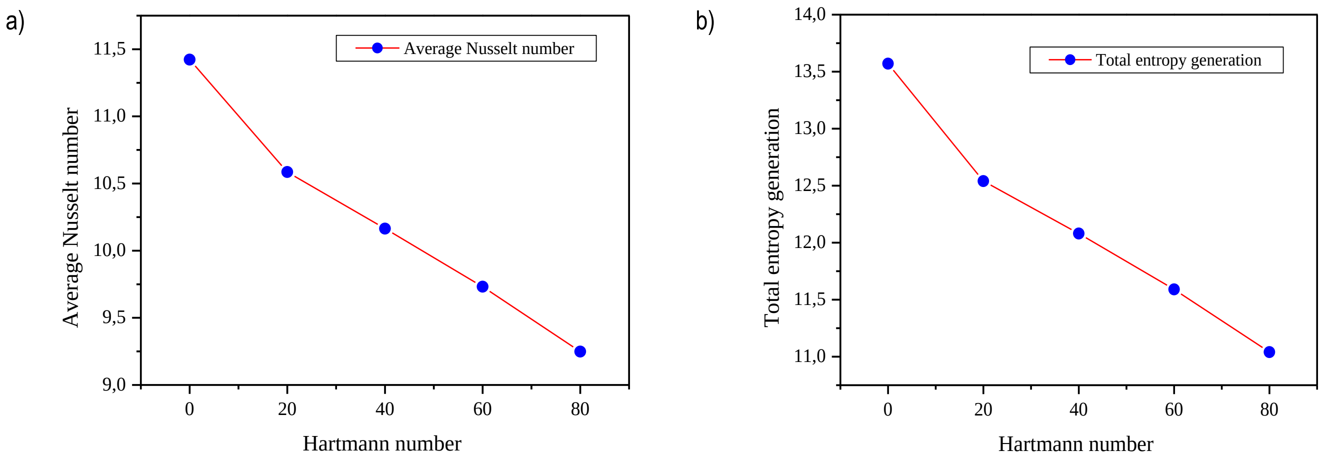

Fig. 9. Num (a) and total Sgen (b) for different values of Hartmann number at Re = 100, Ri = 20, γ = α = 0 and ϕ = 4 · 10^{-2}

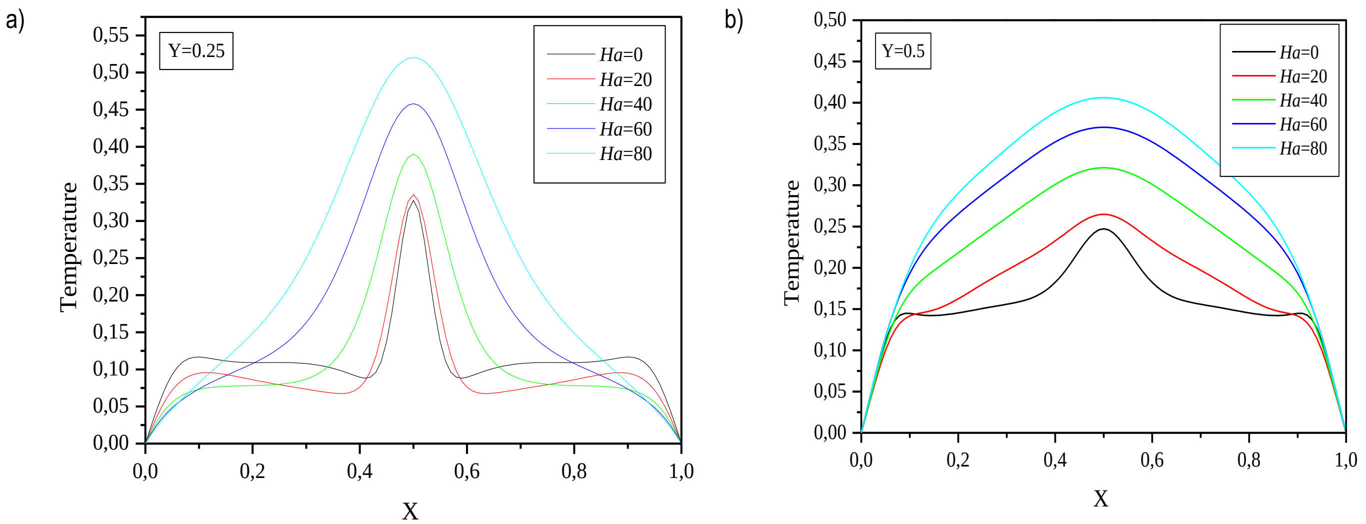

Fig. 10. Temperature variation in the middle of the cavity (a) Y = 0.25 and (b) Y = 0.5 for different values of Hartmann number at Re = 100, Ri = 20, γ = α = 0 and ϕ = 4 · 10^{-2}

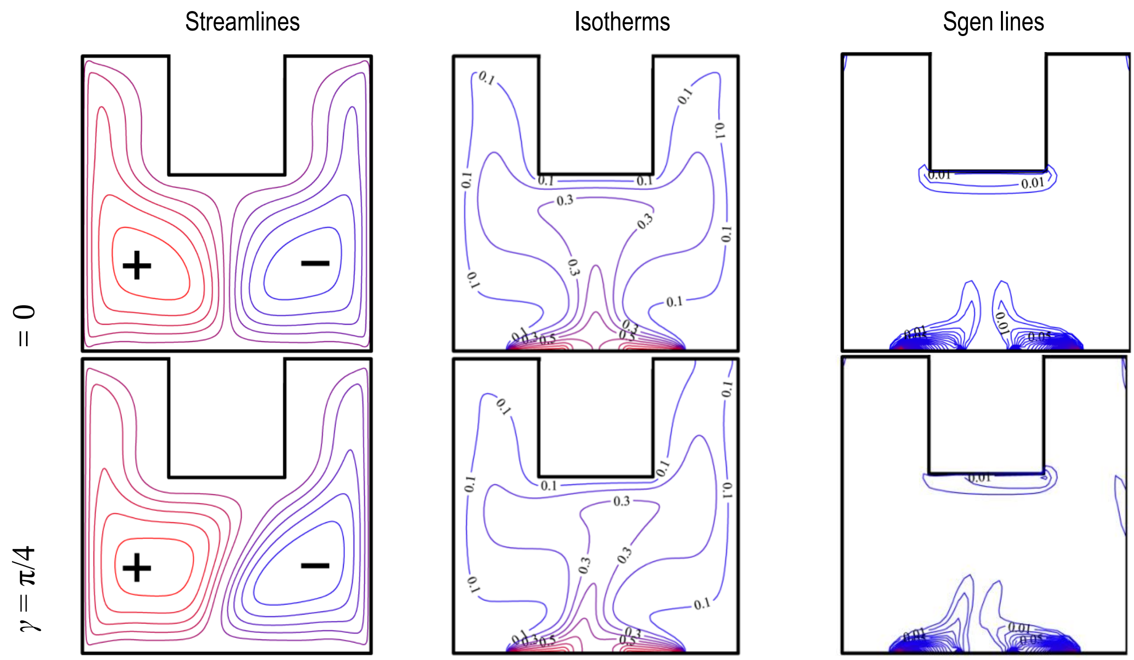

DOI 10.2478/ama-2023-0013

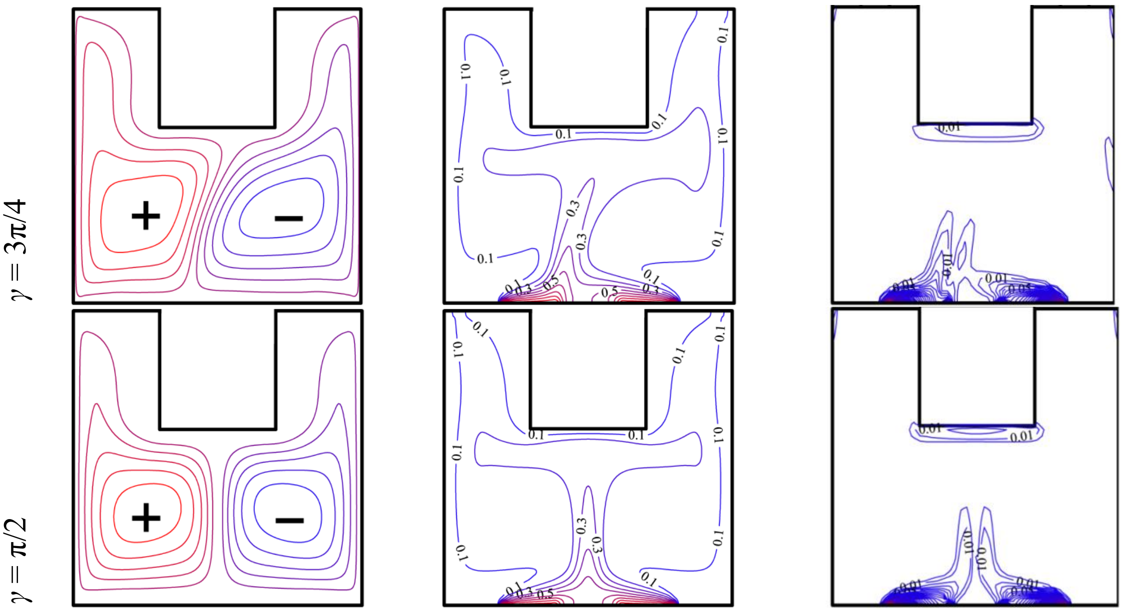

Fig. 11. Streamlines, isotherms and Sgen lines for different γ at α = 0, Re = 50, Ri = 20, Ha = 0 and ϕ = 4 · 10^{-2}

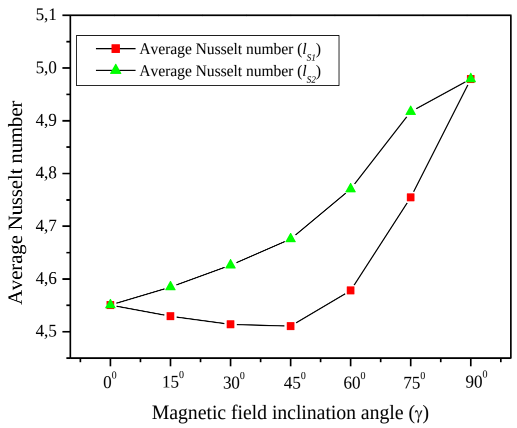

Fig. 12. Num for different γ at α = 0, Re = 50, Ri = 20, Ha = 0 and ϕ = 4 · 10^{-2}

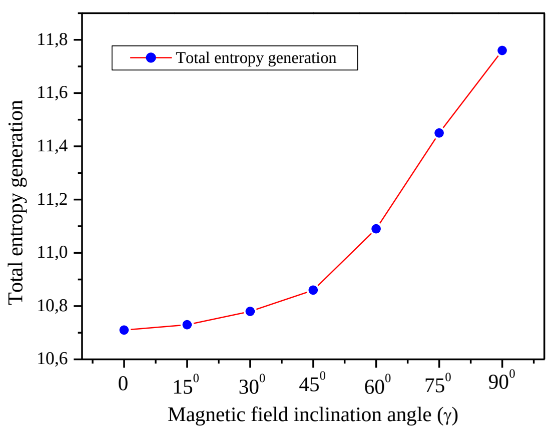

Fig. 13. Total Sgen for different γ at α = 0, Re = 50, Ri = 20, Ha = 0 and ϕ = 4 · 10^{-2}

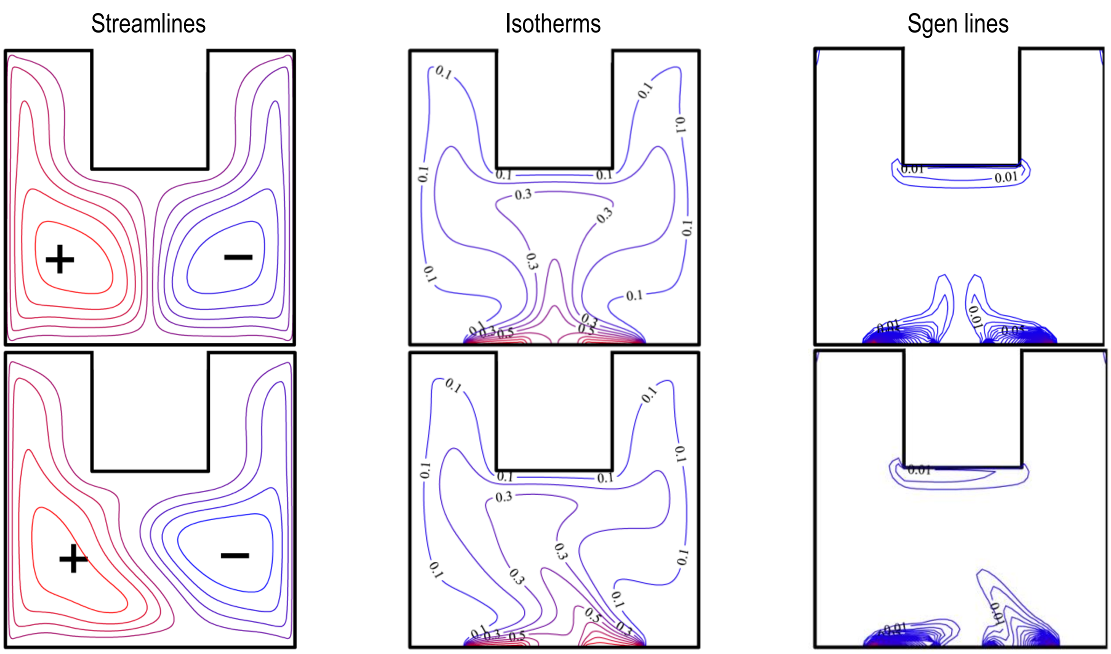

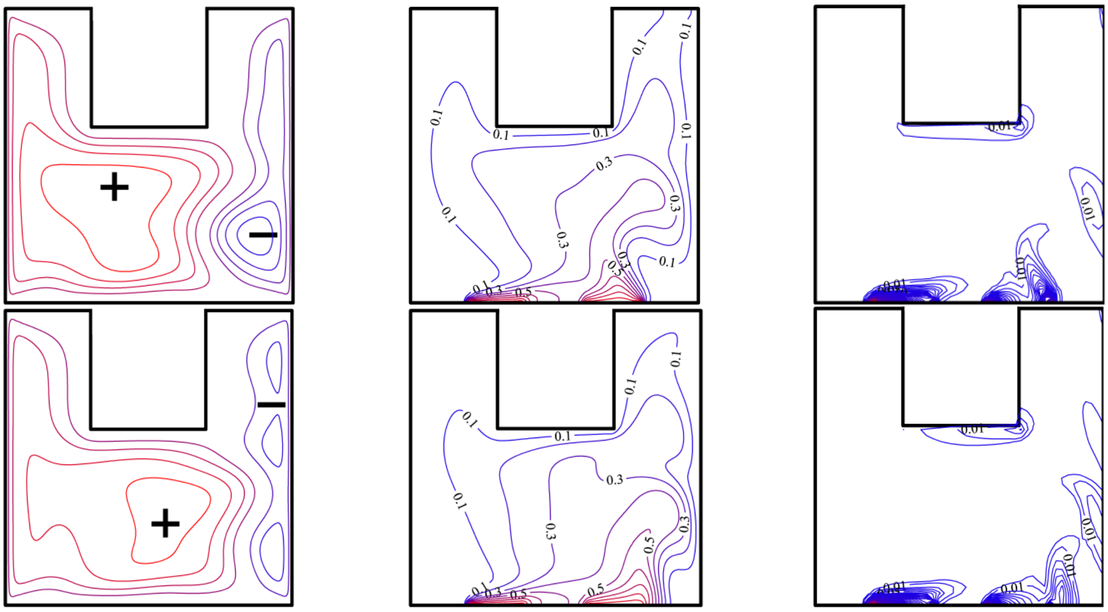

Fig. 14. Streamlines, isotherms and Sgen lines for different α at γ = 0, Re = 50, Ri = 20, Ha = 0 and ϕ = 4 · 10^{-2}

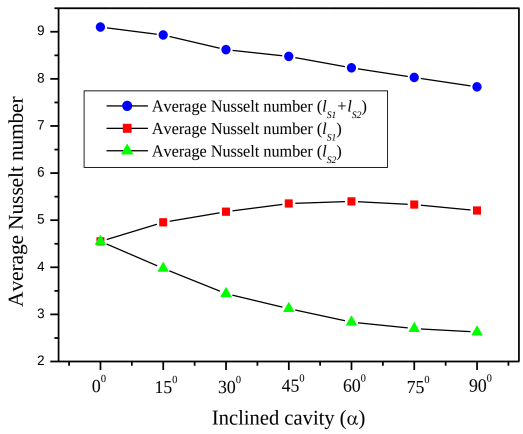

Fig. 15. Num for different α at γ = 0, Re = 50, Ri = 20, Ha = 0 and ϕ = 4 · 10^{-2}

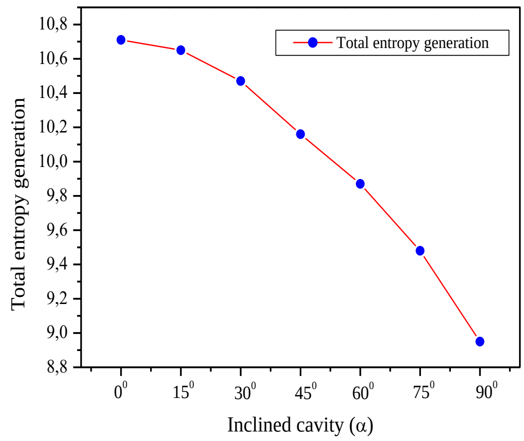

Fig. 16. Total Sgen for different α at γ = 0, Re = 50, Ri = 20, Ha = 0 and ϕ = 4 · 10^{-2}

7. CONCLUSIONS

The novelty of this research consists in the fact that it identifies, and briefly discusses, the physics parameters that have the greatest influence on MHD mixed convection heat transfer of magnetic nanoliquid (CuO/H2O) in a double-lid–driven U-shaped enclosure with discrete heating. Shortly, I will study the impact of the radiation and electric field effects on the unsteady mixed convection three-dimensional stagnation.

Key findings from this numerical study can be summarised as following:

Complex interaction between the various physical phenomena characterising this problem including the natural convection, the shear forces and the magnetic field has been observed.

The Num and the total Sgen augment with Re, ϕ and γ. On the contrary, they decrease with Ha and α.

The maximum value of |ψ|max was obtained for Re = 100.

The maximum heat flow occurs in the centre of the U-shaped enclosure.

The maximum value of |ψ|max was in an indirect relation with Hartmann number.

The optimum magnetic field and U-shaped enclosure inclination angles to maximise heat transfer are γ = 90° and α = 0.

Besides, the excellent utility and effectiveness of the LBM have been demonstrated through our experiences pertaining to its use for the investigation of several CFD and CHT problems, such as turbulent atmospheric plasma spraying jets [42–44], natural convection in confined media in regular and irregular polygons using different LBM models [45–48], MHD and porous media [49–51] and boundary layers flows [52], as well as micro flows in slip regimes [53]. Our future research works will focus on the study of pulsed and turbulent flows using the LBM method. Such problems and conditions can improve the energy efficiency of small-scale systems.

Nomenclature:

B	Magnetic field (Tesla = N/[A · m^2])
c	Lattice speed
c_s	Speed of sound

c_i	Discrete particle speed
c_p	Specific heat ($J \cdot kg^{-1} \cdot K^{-1}$)
F_i	External forces (N)
Ha	Hartmann number
k	Thermal conductivity ($W \cdot m^{-1} \cdot K^{-1}$)
Nu_m	Average Nusselt number
Nu	Local Nusselt number
P	Pressure (Pa)
Pr	Prandtl number
Ra	Rayleigh number
S_{gen}	Entropy generation
Re	Reynolds number
Ri	Richardson number
T	Temperature (K)
u	Horizontal component of velocity ($m \cdot s{-}1$)
v	Vertical component of velocity ($m \cdot s{-}1$)
x, y	Lattice coordinates (m)
L	Height of cavity (m)
	Greek letters
α	Thermal diffusivity ($m2 \cdot s{-}1$)
β	Thermal expansion coefficient ($K{-}1$)
ϕ	Solid volume fraction
μ	Dynamic viscosity ($kg \cdot m{-}1 \cdot s{-}1$)
ρ	Fluid density ($kg \cdot m{-}3$)
θ	Dimensionless temperature
ν	Kinematic viscosity ($m2 \cdot s{-}1$)
σ	Electrical conductivity ($(\Omega m){-}1$)
ψ	Stream function ($m2 \cdot s{-}1$)
	Subscripts
Tc	Cold temperature
Th	Hot temperature

REFERENCES

1. Khan J A, Mustafa M, Hayat T, Alsaedi A. Three-dimensional flow of nanofluid over a nonlinearly stretching sheet: An application to solar energy. Int. J. Heat Mass Transfer. 2015; 86:158-164.
2. Ganvir B, Walke V, Kriplani M. Heat transfer characteristics in nanofluid-A review. Rene. Sust. Energy Reviews. http://dx.doi.org/10.1016/j.rser.2016.11.010
3. Bigdeli MB, Fasano M, Cardellini A, Chiavazzo E, Asinari P. A review on the heat and mass transfer phenomena in nanofluid coolants with special focus on automotive applications. Rene. Sust. Energy Reviews. 2016;60:1615–1633.
4. Assel S, Shan Y, Jiyun Z, Wu J M, Leong KC. Optimization and comparison of double-layer and double-side micro-channel heat sinks with nanofluid for power electronics cooling. Applied Thermal Engineering. 2014;65:124–34.
5. Rafati M, Hamidi AA, Niaser S. Application of nanofluid in computer cooling systems (heat transfer performance of nanofluid). Applied Thermal Engineering. 2012;45:9–14.
6. Yuan LC, Chang WJ, Chieh CT. Analysis of suspension and heat transfer characteristics of Al2O3 nanofluid prepared through ultrasonic vibration. Appl Energy. 2011;88:4527–33.
7. Şahin S, Demir H. Numerical Solution Of Natural Convective Heat Transfer Under Magnetic Field Effect. Acta Mechanica et Automatica. 2019;13(1).
8. Xuan Y, Duan H, Li Q. Enhancement of solar energy absorption using a plasmonic nanofluid based on TiO2/Ag composite nanoparticles. R.S.C. Adv. 2014; 4: 16206.
9. Bhosale GH, Boiling CHF. Enhancement with Al2O3–CuO/H2O hybrid nanofluid, Int. J. Eng. Res. Technol. 2013; 2:946–50.
10. Selvakumar P, Suresh S. Use of Al2O3–Cu/water hybrid nanofluid in an electronic heat sink, IEEE Trans. Compon. Packag. Manuf. Technol. 2 (2012) 1600–7.
11. Duangthongsuk W, Wongwises S. An experimental study on the heat transfer performance and pressure drop of TiO2-water nanofluids flowing under a turbulent flow regime. Int. J. Heat Mass Transfer. 2010; 53:334–44.
12. Sundar LS, Naik MT, Sharma KV, Singh MK, Siva Reddy TC. Experimental investigation of forced convection heat transfer and friction factor in a tube with Fe3O4 magnetic nanofluid. Exp. Therm. Fluid. Sci. 2012; 37:65–71.
13. Aljabair S. Review of computational multi-phase approaches of nano-fluids filled systems. Thermal Science and Engineering Progress. 2022; 28: 101175.
14. Mliki B, Belgacem N, Abbassi M A, Kamel G, Omri A, Entropy Generation and Heat Transfer of Cu–Water Nanofluid Mixed Convection in a Cavity. Int. J. of Mech. Aero. Ind. Mecha. and Manufa. Engin. 2014; 8:2237–2143.
15. Sheremet MA, Pop I. Mixed convection in a lid-driven square cavity filled by a nanofluid: Buongiorno mathematical model. Applied Mathematics and Computation. 2015; 266: 792-808.
16. Nayak RK, Bhattacharyya S, Pop I. Numerical study on mixed convection and entropy generation of Cu–water nanofluid in a differentially heated skewed enclosure. Int. J. Heat Mass Transfer. 2015; 85: 620–634.
17. Sourtiji E, Bandpy MG, Ganji D, Hosseinizadeh S. Numerical analysis of mixed convection heat transfer of Al2O3-water nanofluid in a ventilated cavity considering different positions of the outlet port. Powder Technology. 2014; 262:71-81.
18. Toumi M, Bouzit M, Bouzit F, Mokhefi A. MHD Forced Convection Using Ferrofluid Over A Backward Facing Step Containing A Finned Cylinder. Acta Mechanica et Automatica . DOI: 10.2478/ama-2022-0009 (2021).
19. Djebali R. Mesoscopic study of mixed convection and heat transfer due to crescent shape hot source under magnetic field and Joule effect. Romanian Reports in Physics. 2021; 72: 106.
20. Ali SA , Sahira LE, Alesbe I. Mixed convection in sinusoidal lid driven cavity with non-uniform temperature distribution on the wall utilizing nanofluid. Heliyon. 2021; 7(5):06907.
21. Moumni H, Welhezi H, Djebali R, Sediki E. Accurate finite volume investigation of nanofluid mixed convection in two-sided lid driven cavity including discreteheat sources. Applied Mathematical Modelling. 2015; 39 : 4164-4179.
22. Aljabair S, Mohammed AA, Alesbe I. Natural convection heat transfer in corrugated annuli with H2O-Al2O3 nanofluid. 2020; 6(11): e05568A.
23. Mahmoudi H, Pop I, Shahi M. Efect of magnetic feld on natural convection in a triangular enclosure flled with nanofuid. Int. J. of Termal Sciences. 2012; 59 :126–140.
24. Mliki B, Abbassi M A, Omri A, Zeghmati B. Effects of nanoparticles Brownian motion in a linearly/sinusoidally heated cavity with MHD natural convection in the presence of uniform heat generation/ absorption. Powder Technology. 2016; 295: 69–83.
25. Alesbe I, Ibrahim SH, Aljabair S. Mixed convection heat transfer in multi-Lid- driven trapezoidal annulus filled with hybrid nanofluid. Journal of Physics: Conference Series. 2021; 1973:012065.
26. Hussain S, Mehmood K, Sagheer M. MHD mixed convection and entropy generation of water-alumina nanofluid flow in a double lid driven cavity with discrete heating. J of Magn. and Magn. Mater. DOI: 10.1016/j.jmmm.2016.06.006, 2016.

27. Shirvan KM, Mamourian M, Mirzakhanlari S, Moghiman M. Investigation on effect of magnetic field on mixed convection heat transfer in a ventilated square cavity, Procedia Engineering 127 (2015) 1181-1188.
28. Pordanjani AH, Aghakhani S. Numerical Investigation of Natural Convection and Irreversibilities between Two Inclined Concentric Cylinders in Presence of Uniform Magnetic Field and Radiation. Heat Transfer Engineering. 2021: 1-21.
29. Aghakhania S , Pordanjani AH, Afrand M, Farsani A K, Karimi N, Sharifpur M. Entropy generation and exergy analysis of Ag–MgO/ water hybrid nanofluid within a circular heatsink with different number of outputs. International Journal of Thermal Sciences. 2023; 184: 107891.
30. Mliki B, Abbassi MA, Omri A, Zeghmati B. Lattice Boltzmann analysis of MHD natural convection of CuO-water nanofluid in inclined C-shaped enclosures under the effect of nanoparticles Brownian motion. Powder Technology. doi: 10.1016/j.powtec.2016.11.054
31. Kumar A, Singh AK, Chandran P, Sacheti NC. Effect of perpendicular magnetic field on free convection in a rectangular cavity. Sult. Qa. Uni. J. for Sc. 2015; 20(2):149-59.
32. Mliki B, Abbassi MA, Omri A, Zeghmati B. Augmentation of natural convective heat transfer in linearly heated cavity by utilizing nanofluids in the presence of magnetic field and uniform heat generation/absorption. Powder Technology. 2015; 284:312–325.
33. Mliki B, Abbassi MA, Omri A. Lattice Boltzmann simulation of natural convection in an L-shaped enclosure in the presence of nanofluid. Eng. Sc. and Tech. an Int. J. 2015;18:503–511.
34. Mliki B, Abbassi MA, Omri A. Lattice Boltzmann Simulation of MHD Double Dispersion Natural Convection in a C-shaped Enclosure in the Presence of a Nanofluid. F. Dyn. and Mat. Proce. 2015;11(1): 87-114.
35. Mliki B, Abbassi MA, Omri A, Zeghmati B. Effectsof nanoparticles Brownian motion in a linearly/sinusoidally heated cavity with MHD natural convection in the presence of uniform heat generation/ absorption. Powder Technology. 2016; 295:69–83.
36. Brinkman HC. The viscosity of concentrated suspensions and solutions. Journal of Chemical Physics. 1952; 20 :571-581.
37. Qian YH, Humières D, Lallemand P. Lattice BGK models for Navier-Stokes equation. Europhysics Letters (Epl)). 1992; 17(6): 479.
38. Peng Y, Shu C, Chew YT. Simplified thermal lattice Boltzmann model for incompressible thermal flows. Physical Review. 2003; 68(2): 026701.
39. Ghasemi B, Aminossadati SM, Raisi A. Magnetic field effect on natural convection in a nanofluid-filled square enclosure. Int. J. Therm. Sci. 2011; 50:1748–1756.
40. Lai FH, Yang YT. Lattice Boltzmann simulation of natural convection heat transfer of Al2O3/water nanofluids in a square enclosure, Int. J. Therm. Sci. 2011; 50:1930-1941.
41. Talebi F, Mahmoudi AH, Shahi M. Numerical study of mixed convection flows in a square lid-driven cavity utilizing nanofluid. International Communications in Heat and Mass Transfer. 2010; 37 : 79–90.
42. Djebali R, Ganaoui ME, Pateyron B. A lattice Boltzmann-based investigation of powder in-flight characteristics during APS process. part I: Modelling and validation. Progress in Computational Fluid Dynamics. 2012; 12 (4):270-278.
43. Djebali R, Ganaoui ME, Pateyron B. A lattice Boltzmann based investigation of powder in-flight characteristics during APS process; part II: Effects of parameter dispersions at powder injection. Surface and Coatings Technology. 2013; 220: 157-163.
44. Djebali R, Elganaoui M, Jaouabi A, Pateyron B. Scrutiny of spray jet and impact characteristics under dispersion effects of powder injection parameters in APS process; International Journal of Thermal Sciences, 100(2016), pp. 229-239.
45. Naffouti T, Djebali R. Natural convection flow and heat transfer in square enclosure asymetrically heated from below: A lattice Boltzmann comprehensive study. Computer Modeling in Engineering and Sciences, 2012; 88 (3):211-227.
46. Abbassi MA, Djebali R, Guedri K. Effects of heater dimensions on nanofluid natural convection in a heated incinerator shaped cavity containing a heated block. Journal of Thermal Engineering. 2018; 4 (3):2018-2036.
47. Abbassi MA, Safaei MR, Djebali R, Guedri K, Zeghmati B, Alrashed AA. LBM simulation of free convection in a nanofluid filled incinerator containing a hot block. Int. Journal of Mechanical Sciences. 2018; 148:393-408.
48. Djebali R, Jaouabi A, Naffouti T, Abboudi S. Accurate LBM appraising of pin-fins heat dissipation performance and entropy generation in enclosures as application to power electronic cooling. International Journal of Numerical Methods for Heat and Fluid Flow. 2020; 30 (2):742-768.
49. Djebali R, ElGanaoui M, Naffouti T. A 2D Lattice boltzmann full analysis of MHD convective heat transfer in saturated porous square enclosure. Computer Modeling in Engineering and Sciences. 2012; 84 (6):499-527.
50. Djebali R. Numerical analysis of nanofluid cooling efficiency of hot multishaped cylinder in vertical porous channel; Romanian Journal of Physics, 65, 122 (2020).
51. Ferhi M, Djebali R, Mebarek-Oudina F, Nidal H, Abboudi S. MHD free convection through entropy generation analysis of eco-friendly nanoliquid in a divided L-shaped heat exchanger with LBM simulation. Journal of Nanofluids. 2022; 11 (1):99–112.
52. Ferhi M, Djebali R. Appraising conjugate heat transfer, heatlines visualization and entropy generation of Ag-MgO/H2O hybrid nanofluid in a partitioned medium. International Journal of Numerical Methods for Heat and Fluid Flow. 2020; 30(10):4529-4562.
53. Ferhi M, Djebali R. Heat transfer appraising and second law analysis of Cu-water nanoliquid filled microchannel: Slip flow regime. Romanian Journal of Physics. 2022; 67:605.

Acknowledgements: This work was supported by the Tunisian Ministry of Higher Education and Scientific Research under grant Project no: 20/PRD-22.

Bouchmel Mliki: https://orcid.org/0000-0002-0200-8060

Rached Miri: https://orcid.org/0000-0001-9113-5370

Ridha Djebali: https://orcid.org/0000-0002-1017-3410

Mohamed A. Abbassi: https://orcid.org/0000-0002-1915-0944